

# Electron and Hydrogen Atom Transfers in the Hydride Carrier Protein EmoB

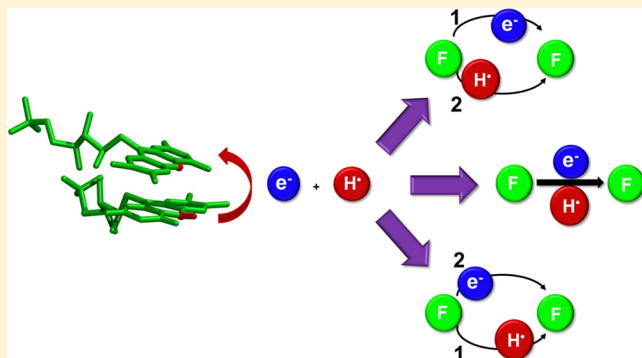
Natacha Gillet\*,†,‡ Bernard Lévy,† Vicent Moliner,‡ Isabelle Demachy,† and Aurélien de la Lande\*,†

†Laboratoire de Chimie-Physique, Université Paris Sud, CNRS, UMR 8000, 15 rue Jean Perrin, 91405 Orsay CEDEX, France

‡Departament de Química Física i Analítica, Universitat Jaume I, 12071 Castellón, Spain

## S Supporting Information

**ABSTRACT:** In this article, we investigate the mechanism of hydride transfer taking place within the EmoB protein of the *Mesorhizobium* species. The reaction involves the net transfer of one proton and two electrons from a reduced flavin mononucleotide (FMN) cofactor, which is anchored in the protein scaffold, to a diffusible oxidized FMN cofactor, both being held together by  $\pi$ -stacking interactions. To analyze the formal hydride transfer in terms of more elementary steps, electron transfer (ET), and hydrogen atom transfers (HAT), we employ a combination of classical molecular dynamics simulations and hybrid constrained Density Functional Theory/Molecular Mechanics (cDFT/MM) energy calculations to build the free energy profiles, for the ET before and after HAT occurs between the flavins. The main outcomes of our study are first to highlight the role of the protein in stabilizing the  $\pi$ -stacked FMN dimer and second to reveal the coupling between the ET and HAT. Before HAT has taken place, ET is unfavorable by 8 kcal/mol and become favorable by 8 kcal/mol after HAT. Our simulations show that such a coupling is not present for the analogous process in water (ET is almost athermal). This suggests a functional role for the protein matrix to ensure EmoB a role of hydride carrier in the *Mesorhizobium* species.



## INTRODUCTION

Hydride transfers are common reactions in chemistry and biology.<sup>1</sup> They involve the transfer of two electrons and one proton between a donor and an acceptor.<sup>2</sup> In biological media, hydride transfers are key steps of catalytic cycles of enzymes belonging to various families such as some dehydrogenases (e.g., alcohol dehydrogenase, flavocytochrome *b2*...), some reductases (e.g., dihydrofolate reductase), or some oxidases (e.g., choline oxidase, glucose oxidase...) to name but a few examples. Molecules such as nicotinamide adenine dinucleotide (NADH), flavin adenine dinucleotide (FAD), flavin mononucleotide (FMN), or dihydrofolate are well-known cofactors carrying hydride equivalents. Under certain physiological conditions the *Mesorhizobium* species produces a monooxygenase (EmoA)<sup>3</sup> that catalyzes ethylene-diamine-tetra-acetic acid (EDTA) degradation. EmoA (EDTA monooxygenase) needs to be supplied with reduced flavin mononucleotide ( $\text{FMNH}_2$ ) to achieve this task. The protein EmoB is thought to be a partner of EmoA by producing  $\text{FMNH}_2$  in a preliminary step. In 2008, a series of X-ray structures was reported by Nissen et al., which helped to uncover the mechanism of reduction of FMN to  $\text{FMNH}_2$  by EmoB.<sup>4</sup> The process requires the participation of two FMN cofactors, one being permanently anchored to the EmoB protein scaffold and one being diffusible, and an NADH cofactor as the initial hydride donor. The process proceeds through a so-called Ping Pong Bi Bi

mechanism meaning that EmoB first catalyzes the reduction of the anchored FMN by NADH, and in a subsequent step, the reduction of the diffusible FMN by the anchored FMN.<sup>4</sup> In this work, we are interested in the hydride transfer within the FMN:FMN oxidoreductase EmoB. One of the X-ray structures reported in ref 3 clearly shows two FMN cofactors, held by  $\pi$ -stacked interactions in an adequate conformation for hydrogen atom transfer between the two N5 nitrogen atoms of the two isoalloxazine rings (Figures 1 and 2).

The hydride transfer terminology actually refers to the net balance of the particle transfers, two electrons and a proton, but does not portray detailed mechanisms by which these particles are transferred. In recent reviews, Hammes-Schiffer classified the various mechanisms for transferring electrons and protons between (eventually distinct) donor and acceptor groups.<sup>6,7</sup> Rate constant expressions have been derived for most of the limit regimes. For a given system, it is essential to clarify which type of physicochemical process is involved in order to choose the most adequate theoretical framework. Our aim is to model the net hydride transfer between the flavin cofactors at the surface of the protein EmoB in terms of more fundamental steps (electron and proton transfers). The conceivable mechanisms are summarized in Figure 3. For the chemical

Received: February 27, 2014

Published: September 26, 2014



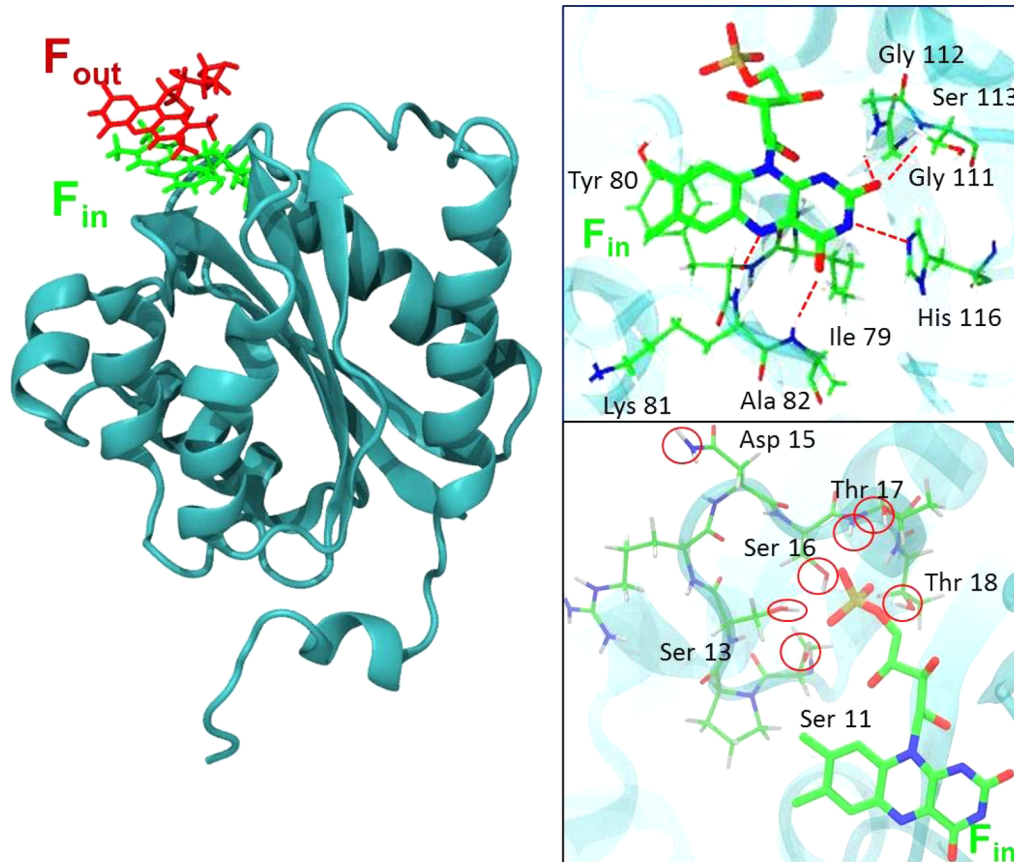


**Figure 1.** Crystallographic structure of the EmoB protein with the two  $\pi$ -stacked flavins  $F_{in}$  and  $F_{out}$  (left) and the hydrogen interactions around the isoalloxazine ring of the protein flavin (red dashed line, top right) and polar residues interacting with the phosphate moiety (red circle, bottom right). (PDB entry: 2VZH).<sup>4</sup> The figures have been drawn with VMD.<sup>5</sup>

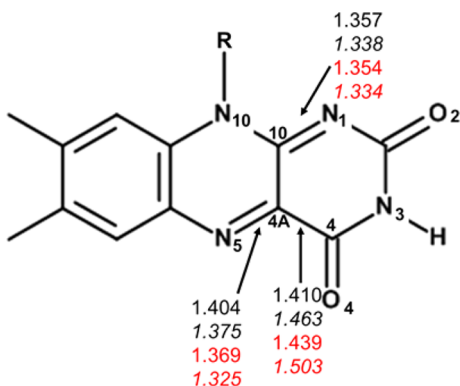


**Figure 2.** Isoalloxazine part of the FMN cofactor (R: d-ribitol-5-phosphate tail). The distances (in Å) correspond to average distances obtained from 6 to 8 ps of cDFT/MM MD simulations for negatively charged (normal font), neutral (italic font), protonated (black), or deprotonated (red) flavins.

system of present interest some of these mechanisms can already be excluded based on qualitative reasoning. For example, a genuine hydride transfer (mechanism a) can be discarded because an actual hydride anion traveling over a few Ångströms between the flavin ions should be oxidized by either of the two flavins. Similarly, the mechanism initiated by an acid–base reaction (mechanism b) seems unlikely because reduced flavins are strong bases while oxidized flavins are strong acids. For similar reasons, mechanism c, which is initiated by a

two-electrons reduction of the right-hand-side flavin, is unlikely because the second electron transfer would produce a high energy intermediate ( $FH^+...F^{2-}$ ). So it seems that the formal hydride transfer requires the respective transfers of a hydrogen atom and of an electron (see also ref 8). In the present case, three alternative mechanisms remain possible (mechanisms d–f). In mechanism d, the process is initiated by an electron transfer, followed by an hydrogen atom transfer, while it is the reverse order in mechanism e. In f, one assumes that the overall process is governed by the transfer of the hydrogen atom while the second electron is comparatively fast. The difference between mechanism d (or e) and f, therefore, stems in the respective time scales of the electron and hydrogen atom transfers. At first glance, mechanism f seems reasonable because the electronic coupling between the diabatic states relevant to ET between two stacked isoalloxazine is probably large, thereby placing the ET in the electronically adiabatic regime. However, ETs involving flavin cofactors can involve large reorganization energies,<sup>9,10</sup> which, according to the Marcus theory,<sup>11</sup> can lead to significant free energy barriers despite the large amplitude of the coupling. Therefore, ET may not be so fast compared to HAT so that mechanisms e and d may compete with mechanism f. The objective of the present study is to investigate mechanisms (d–f) in the case of the formal hydride transfer within the protein EmoB.

This article is divided as follows. In the first section, we detail the methodology we have followed and give the practical computational details. In the second section, we present results of the investigation of the net hydride transfer between the

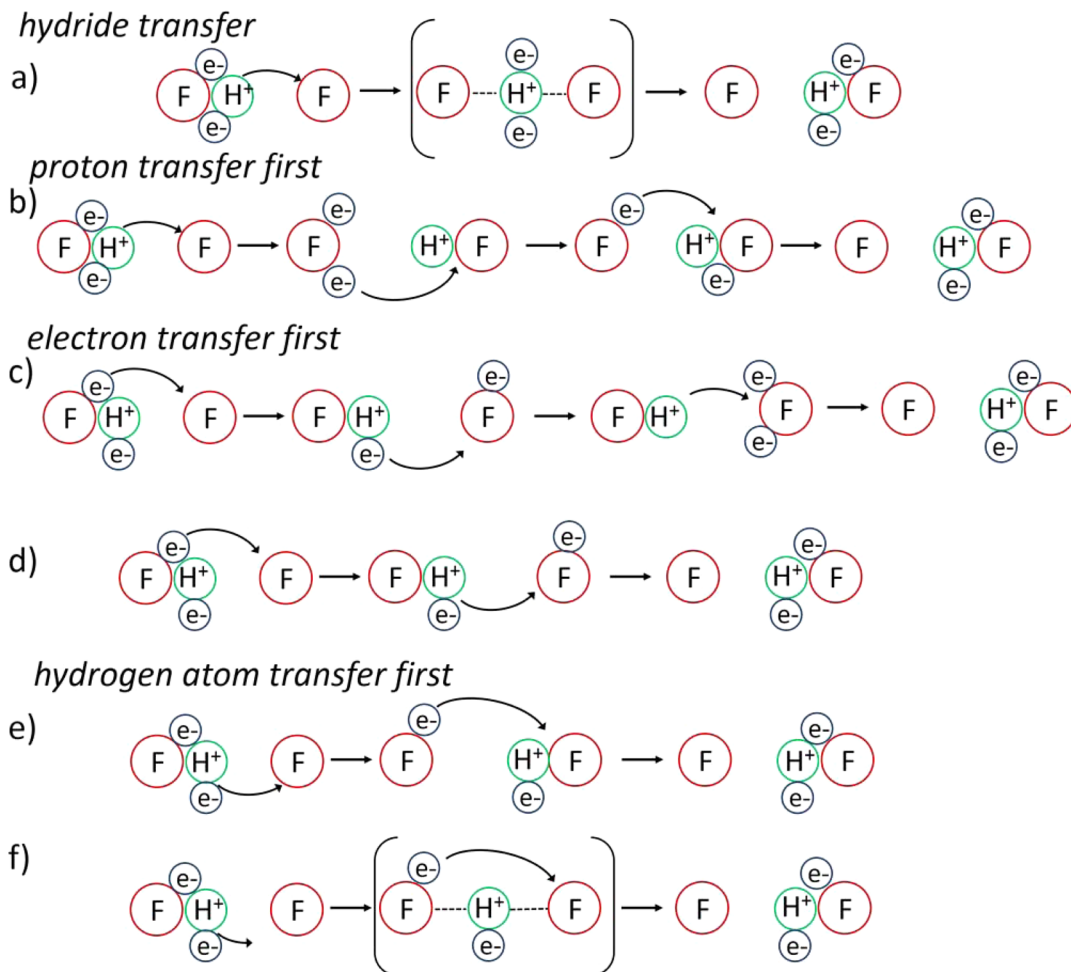


**Figure 3.** Decomposition of a net hydride ion transfer between a donor and an acceptor (in the present study these are two flavin cofactors, F) in terms of elementary steps. (a) genuine hydride transfer, (b) mechanism initiated by an acid–base reaction, (c, d) mechanism initiated by an electron transfer, (e, f) mechanisms initiated by an hydrogen atom transfer.

FMN cofactors within EmoB and in water, thereby highlighting the effect the protein matrix.

## I. METHODOLOGY

**I.1. Theoretical Framework for Establishing the ET Free Energy Profiles.** Initial insight into mechanisms d–f may be obtained by determining the free energy profiles for the ET before and after the HAT taking place. Throughout this article,  $F_{\text{in}}$  will denote the FMN cofactor anchored in the EmoB.  $F_{\text{in}}$  carries the hydride ion in the reactant state.  $F_{\text{out}}$  will denote the external flavin that receives the hydride ion from  $F_{\text{in}}$ . To obtain the ET energy profiles, we have worked in the framework of the Marcus Theory, the validity of which will be tested in the Results section. The construction of free energy curves for ET from atomistic simulations is now well established,<sup>12</sup> and the reader is referred for example to refs 13, 14, or 15 for delineated descriptions of these approaches. For clarity, we only summarize here the main lines of the procedure.

To begin, let us first recall that ETs usually involve structural modifications of both the inner-structures of the redox partners (bond lengths, angles, ...) and of the molecular environment (solvent, protein, ...).<sup>16</sup> Therefore, a suitable reaction coordinate has to take into account the extremely large number of degrees of freedom reflecting the progress of the reaction.

The energy gap between the electronic states characterizing the electron transfer has proven to be an efficient global reaction coordinate.<sup>17</sup> In the framework of the Marcus Theory, and considering for illustrative purpose the ET between two flavins, the two electronic states just mentioned would be two diabatic states for which the electron is localized either on one flavin (for example in the initial state) or on the other (the final state). The Helmholtz free energy for state x (initial or final states), as a function of the energy gap  $\Delta E = (E_f - E_i)$  is given by

$$A_x(\Delta E) = -k_B T \ln(p_x(\Delta E)) + C_x \quad (1)$$

where  $p_x(\Delta E)$  is the probability distribution of the diabatic energy gap,  $T$  is the temperature,  $k_B$  is the Boltzmann constant, and  $C_x$  is a constant. To determine the functions  $A$  by numerical simulations, a methodology providing an adequate balance between the accuracy of the energy gap  $\Delta E$  evaluation coupled to the most extensive sampling of the conformational space (for evaluating  $p_x(\Delta E)$ ) is required. An examination of the recent literature dealing with the modeling of flavin redox properties shows that different strategies have been followed by various authors. Kiliç and Ensing<sup>7</sup> reported a study of the first and second one-electron reductions of lumiflavin in water based on first-principles DFT Born–Oppenheimer Molecular Dynamics simulations (DFT-BOMD). The method permits an

accurate calculation of the underlying potential energy surface (PES). In particular, the bending of the flavin in the fully reduced form (the so-called “butterfly” deformation) is well reproduced by DFT. On the other hand, the cost of DFT-BOMD limits the simulation lengths to a few tens of picoseconds. Although this time scale is probably acceptable for simulating lumiflavin in water, it might not be sufficient for modeling similar redox properties within a protein such as Emob. In fact, proteins are characterized by multiscale dynamics including motions much slower than the picosecond time scale that still can enter the reaction coordinates of ET reactions. In 2007, Bhattacharyya et al.<sup>18</sup> carried out MD simulations based on PES calculated with a hybrid Self-Consistent-Charge-Tight-Binding-DFT(SCC-DFTB)/Molecular Mechanics approach. The method was applied to evaluate the redox potentials of lumiflavin in water or of the FAD cofactor embedded in the medium-chain acyl-CoA dehydrogenase and in the cholesterol oxidase enzymes. MD simulations of several nanoseconds are achievable with semiempirical quantum mechanical methods. Finally, a frequent strategy found in the literature is to couple the realization of MD simulations using a MM force field, to the a posteriori evaluation of the energies with a more accurate method on snapshots extracted from the trajectories.<sup>15,19</sup> This is the strategy followed in this work. Because of the use of a classical force field, a main advantage of this procedure is that rather extensive conformational sampling of the protein can be achieved (several hundreds of nanoseconds). The details of the computational protocol will be given in the next two subsections. For the moment, we continue describing the procedure for establishing Marcus Theory energy profiles.

Once the diabatic energy gaps have been sampled on the PESs of each electronic state, the probability distributions  $p_i(\Delta E)$  and  $p_f(\Delta E)$  can be evaluated. If these are Gaussian with similar widths  $\sigma_i$  and  $\sigma_f$  (which is an underlying hypothesis of the Marcus theory), the diabatic free energy curves are parabolic functions having the same curvatures. The reaction free energy and the reorganization energy of a given ET reaction can be obtained through a linear response approximation (LRA) by

$$\Delta A_{i \rightarrow f}^{\circ} = \frac{1}{2}(\langle \Delta E \rangle_i + \langle \Delta E \rangle_f) \quad (2)$$

$$\lambda_{i \rightarrow f} = \frac{1}{2}(\langle \Delta E \rangle_i - \langle \Delta E \rangle_f) \quad (3)$$

The angular brackets denote the canonical average. The average energy gap is used to calculate the diabatic free energy of the reaction with eq 1, which gives the bottom of the parabolic curves. With  $\Delta E$  taken as the reaction coordinate, it can be shown by LRA that, for any value of  $\Delta E$ , one has  $\Delta A^{\circ}(\Delta E) = \Delta E$ .<sup>10,11,20,21</sup> This permits us to build supplementary points for one state from the points obtained for the other state. The parabolic curve of one state is fitted on these two sets of points. Finally, the curves are vertically positioned by setting the constant  $C$  in eq 1 to 0 for the function  $A_i$  (initial state) and to  $\Delta A^{\circ}$  for the function  $A_f$  (final state). To plot the curves corresponding to the adiabatic states, we assume that for a given diabatic energy gap value, the mean value of the energy of the two adiabatic states equals the mean of the energy of the two diabatic states.

**I.2. Calculation of Diabatic Energies.** The determination of  $\Delta A_{i \rightarrow f}^{\circ}$ ,  $\lambda_{i \rightarrow f}$ , and  $A^{\circ}_x$  via eqs 1–3 requires the energy of each

of the diabatic states. ET diabatic states would correspond to electronic states for which the transferred electron is localized either on  $F_{\text{in}}$  or on  $F_{\text{out}}$ . We have used the constrained DFT approach (cDFT) to define such ad hoc diabatic states. To avoid confusion, we state that, in this article, the term “constrained DFT” refers to the method introduced by Dederichs et al.<sup>22</sup> and further developed by Wu and Van Voorhis.<sup>23</sup> This cDFT approach provides a means to impose the charge on particular fragments of a molecular system. To this end, a Lagrange multiplier scheme is employed to introduce a charge constraint in the total DFT functional. The value of the Lagrange multiplier is optimized on-the-fly during the Self-Consistent-Field procedure.<sup>23</sup> The reader is referred to review articles or book chapters for details on cDFT.<sup>24,25</sup> cDFT calculations have been performed with the program deMon2k.<sup>26,27</sup> In the present case, we have imposed a net charge difference of  $\pm 1.0$  between the two isoalloxazine groups to define the initial and final states. The transferred hydrogen atom was not part of the constrained domains. Obviously, since atomic charges cannot be uniquely defined in quantum mechanics, a choice for partitioning the electron density when imposing the charge difference in cDFT has to be made. We have tested various population analyses and found that the Hirshfeld scheme gives the most satisfying description of the diabatic states of ET between the FMN cofactors (see Supporting Information).

The Coulomb and exchange-correlation (XC) potentials have been calculated using auxiliary basis sets to fit the electronic density.<sup>28</sup> The XC energy has been calculated numerically with the Perdew–Becke–Ernzerhof functional<sup>29</sup> and using an adaptive grid of medium accuracy.<sup>30</sup> The long-range Coulomb integrals were calculated through a multipolar expansion scheme.<sup>31</sup> The DZVP-GGA atomic basis set (double- $\zeta$  with polarization functions atomic orbital basis set calibrated for Generalized-Gradient-Approximation XC functional)<sup>32</sup> has been used to expand the molecular orbital functions and the GEN-A2 auxiliary basis set to expand the auxiliary electronic densities. The DFT energies are corrected by the empirical expression proposed by Goursot et al. to account for dispersion.<sup>33</sup> The C6 coefficients entering the empirical expression were taken from ref 34.

To include explicitly the environment of the isoalloxazine rings, we have used a hybrid cDFT/MM approach.<sup>35</sup> The QM/MM energy expression is calculated via a subtractive scheme:<sup>36</sup>

$$E_{F_{\text{in}}F_{\text{out}}+\text{env}}^{\text{cDFT/MM}} = E_{F_{\text{in}}F_{\text{out}}+\text{env}}^{\text{MM}} - E_{F_{\text{in}}F_{\text{out}}}^{\text{MM}} + E_{F_{\text{in}}F_{\text{out}}}^{\text{cDFT}} \quad (4)$$

In this expression,  $E_A^X$  denotes the energy of system A (that is, the two stacked flavins isolated or in their environment) at the level of computation X (MM or cDFT). The atoms treated at the QM level are those of isoalloxazine rings and the methyl groups connecting the aromatic cycles to the ribitol moieties. The frontier between the QM and MM regions is treated by the link atom ( $H_L$ ) method. The length of the C–H<sub>L</sub> bond has been parametrized in a preliminary DFT optimization. The calculation of cDFT/MM energies are carried out by interfacing deMon2k and the MM software CHARMM<sup>37</sup> through the software Cuby developed by Řežáč.<sup>38</sup>

For a given conformation of the nuclei, two cDFT calculations are carried out to evaluate the diabatic energy gap. The electronic coupling ( $H_{if}$ ) between the diabatic states is also calculated according to the procedure described in ref 39.

The diabatic Hamiltonian is diagonalized to obtain adiabatic energies.

**I.3. Inclusion of Electronic Polarizability.** It has been shown on several occasions that one should take into account the electronic polarizability of the environment when building the free energy profile for ET transfer reactions, particularly in the adiabatic regime.<sup>13,15,40,41</sup> Inclusion of electronic polarizability in biomolecular simulations still represents a challenge even though various strategies have been proposed.<sup>42,43</sup> Estimates of the driving force and of the reorganization energies including electronic polarizability were obtained with the AMBER ff02.r1 polarizable force field.<sup>44</sup> The method employs a point dipole model whereby the polarization energy arise from the interaction between the partial charges and the induced dipoles on each atom. An iterative self-consistent scheme is used to converge the induced dipoles. The isoalloxazine rings were made nonpolarizable to make this scheme compatible with the QM/MM energy expression (eq 4). Because of the high computational cost of MD simulations with polarizable force fields, we calculated polarized energies on the geometry ensembles obtained from MD simulations with the nonpolarizable FF.

**I.4. System Preparation and Calibration of the Force Field.** We have started our study with the X-ray structure of EmoB resolved at 2.5 Å and reported by Nissen et al. (Protein Data Bank entry: 2VZH).<sup>3</sup> In this structure, the two isoalloxazine rings of the FMN cofactors are stacked together in a favorable position for the hydride transfer reaction (Figure 1). The hydrogen atoms have been added with the HBUILD module of the CHARMM program at pH 7 and after computing the pK<sub>a</sub> values of ionizable residues with PROPKA software.<sup>45</sup> The protein atoms are treated with the CHARMM 27 force field with CMAP corrections, and the water are treated with the flexible SPC model.<sup>46</sup> The two diabatic states characterizing ET from F<sub>in</sub> to F<sub>out</sub> before HAT are denoted {F<sub>in</sub>H<sup>-</sup>,F<sub>out</sub>} and {F<sub>in</sub>H,F<sub>out</sub><sup>-</sup>}. After HAT, the diabatic states are denoted {F<sub>in</sub><sup>-</sup>,F<sub>out</sub>H} and {F<sub>in</sub>F<sub>out</sub>H<sup>-</sup>}.

Specific force field parameters are necessary for each of these diabatic states. Atomic charges of the isoalloxazine rings and the N5–C4A, C4A–C4, N1–C10 bond parameters have been determined (see Figure 2). Only these three bonds have been calibrated to avoid multiplying the number of atom types in the force field and because these are the most sensitive bonds to the changes of redox states.<sup>7</sup> The Lennard-Jones parameters are kept constant for all diabatic states.

The calibration has been carried out on the π-stacked isoalloxazine rings. The partial atomic charges have been fitted to reproduce the electrostatic potential created by the flavins calculated at the DFT level. cDFT was used to calculate the electrostatic potential for the two diabatic states. For each of them, the geometry was first optimized at the cDFT/MM level. Then, the gas phase cDFT electrostatic potential was computed on a grid of points that was generated with a five-layer scheme using the Connolly algorithm.<sup>47</sup> Each layer corresponds to the surface created by atom-centered spheres, the radii of which are multiples of their van der Waals radii (1.4, 1.6, 1.8, 2.0, and 2.2). The charges were fitted by a least-squares method to reproduce the gas phase cDFT electrostatic potential. In the fitting step, we have constrained the hydrogen atoms of each methyl group to have the same charges. We have also imposed smooth harmonic restraints on the charges of every heavy atom to avoid excessively large values. This is a common procedure to avoid excessively large values (for example larger than 1.0 in

absolute value for CHON atoms) and to be trapped in local minima in the fitting procedure. This strategy is followed for instance in the RESP approach (using hyperbolic constraint).<sup>48</sup> It has to be noted that the addition of smooth constraints in the fitting procedure do not alter the quality of the fit as seen from the Relative Root Mean Square Deviation calculated over the grid points between the DFT electrostatic potential and that created by the MM charges. The sets of charges are given in the Supporting Information (Tables S2–S5). They correctly reproduce the dipole moment of the π-stacked isoalloxazine rings calculated at the cDFT level, and the Deviations RRMSD from the cDFT potential is low (<3%). Moreover, for each diabatic state the total charges of the F<sub>in</sub> and F<sub>out</sub> almost equal 0.0 or -1.0. This indicates that the sets of MM charges do in fact correspond to the diabatic states we wish to simulate. Note that we attempted to impose a strict charge difference of ±1.0 by further applying a constraint in the charge fitting step. This was however at the price of degrading the RRMSD or to a less good reproduction of the cDFT dipole moment of the π-stacked flavins. We have not retained these sets of charges.

To set the reference lengths and the force constants of the N5–C4A, C4A–C4, N1–C10 bonds, we have carried out short (few ps: between 6 and 10 ps) ab initio MD simulations at the cDFT/MM level (data not shown) for each diabatic state (Figure 2). The MM force field parameters (reference bond lengths and force constants) were tuned manually in preliminary tests to reproduce at best the average bond lengths and the standard deviations obtained from the cDFT/MM MD simulations.

Classical MD simulations have been performed with the software NAMD (version 2.9).<sup>49</sup> MD simulations were performed within the NPT ensemble using a Langevin approach to control the temperature and the pressure. Long range electrostatic interactions have been computed with the Ewald summation technique using a grid spacing of 1 Å and a cutoff value of 12 Å. We used a multiple time stepping integration scheme as implemented in NAMD to speed-up the MD simulations. The integration time step for propagating the nuclear motions and to calculate the bonded terms of the MM energy function was set to 1 fs. The evaluation of the Lennard-Jones interactions and of the short-range (<12 Å) electrostatic interactions was performed every 2 fs, while the long-range electrostatic interactions were calculated every 4 fs. This combination of 1 fs, 2 fs, and 4 fs is a recommended choice for NPT simulations with flexible hydrogenated bond.<sup>48</sup> The convergence of the mean diabatic energy gap requires few to 15 ns (Supporting Information Figure S1). Supplementary details will be given for every particular simulation in the course of the Results section.

## II. RESULTS

The results section is organized as follows. We first investigate the electron transfer in aqueous solution between a reduced FMN and an oxidized FMN, being held together through π-stacking interactions. We next turn to the EmoB hydride transfer. We investigate the ET energy profiles before and after HAT. The Marcus theory parameters (driving force, reorganization energy, and electronic coupling) are analyzed. Finally, we investigate the actual competition between the ET and HAT (mechanisms e or d vs f, Figure 3).

**II.1. Electron Transfer between FMNs in Water.** For the investigation of ET in solution, we consider the states {FH<sup>-</sup>;F} and {FH;F<sup>-</sup>} (the subscripts in and out, being irrelevant for the

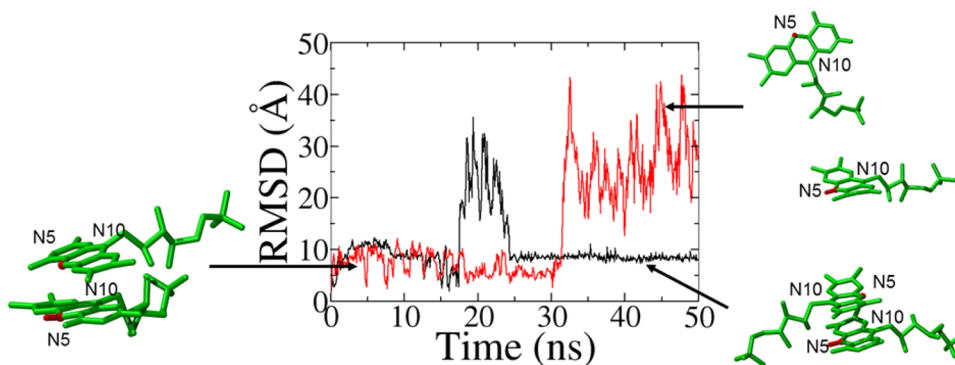


**Figure 4.** Time evolution of the RMSD on heavy atoms of the deprotonated FMN after alignment on the protonated FMN. Black line corresponds to  $\{\text{FH}^-;\text{F}\}$  state and red line to  $\{\text{FH};\text{F}^-\}$ . Large values of RMSD (more than 13 Å) correspond to destacked conformation while small values (around 10 and below) correspond to fluctuations in the stacked complex with rotation of the flavins.

reaction in water, are dropped in this section). The initial structure of the  $\pi$ -stacked isoalloxazines was extracted from the X-ray structure of the protein and solvated in a box of water molecules. When running the MD simulations without any constraints the initial  $\pi$ -stacked geometry of the flavins is lost in a few nanoseconds (Figure 4). For the MD simulation on the  $\{\text{FH}^-;\text{F}\}$  state (black curve), the RMSD fluctuates most of the time around 10 Å. This situation corresponds to  $\pi$ -stacked geometries but in which the N5 atom faces the N10 (see Figure 4). Even though ET may take place in such conformations, the HAT would be impossible because the N5 atoms do not face each other. Larger RMSD values (e.g., >20 Å) correspond to unbound flavins. In such conformations, ET would only take place with an exponentially decreasing rate as long as the FMN cofactors are separated in space. For the MD simulation on the  $\{\text{FH};\text{F}^-\}$  state (red curve), the geometry of the complex fluctuates between the two  $\pi$ -stacked conformations during 30 ns before complete destacking occurs.

Our objective is to compare the energetics of ET between  $\pi$ -stacked isoalloxazine rings in water and in EmoB, in geometries that are also suitable for HAT between the N5 atoms. We thus have applied a constraint during the MD simulations in water to ensure that the isoalloxazine rings remain stacked. After some tests, two harmonic constraints were applied on the N5–N5 and on the N10–N10 distances with reference lengths of 3.5 and 4.5 Å, respectively, which are comparable with mean distances obtained in EmoB MDs (described below). Loose force constants (5 kcal/mol·Å<sup>2</sup>) were applied to ensure that the constraints do not provoke any artifact on structure of the flavins but simply prevent destacking. MD simulations of 100 ns were generated on each state. The energy gap was subsequently sampled every 100 ps at the cDFT/MM level. We will first discuss the date with the nonpolarizable force field. To check the linear response approximation for our system we have plotted in Figure 5 the histograms of the cDFT/MM diabatic energy gap (crosses). They can be well fitted by Gaussian functions with a good correlation coefficient of 0.99 and with comparable standard deviations (5.95 vs 6.15 kcal/mol). This indicates that the linear response approximation can be safely applied to model ET between the FMN cofactors in water and, consequently, that the Marcus Theory is an acceptable theoretical framework in the present case. This is fortunate because the probability to have conformations associated with a null energy gap is extremely low and the free energy of activation  $\Delta A^\ddagger$  cannot be obtained directly from the simulation data. Instead the Marcus relationship between

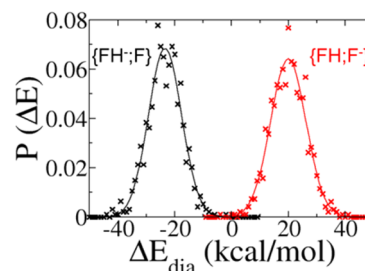


**Figure 5.** Distribution of the vertical diabatic energy gaps for the electron transfer during simulations on state  $\{\text{FH}^-;\text{F}\}$  (black line) or on state  $\{\text{FH};\text{F}^-\}$  (red line). Crosses correspond to the  $p(\Delta E)$  histograms fitted by Gaussian functions in solid lines.

the free energy of the reaction and the reorganization energy  $\Delta A^\ddagger = (\Delta A^\circ + \lambda)^2/4\lambda$  will be used to estimate  $\Delta A^\ddagger$ .

The driving force of the reaction ( $\Delta A^\circ$ ) and the reorganization energy ( $\lambda$ ) calculated with eq 2 and 3 are given in Table 1. The diabatic free energy curves are plotted in

**Table 1. Driving Force ( $\Delta A^\circ$ ) and Reorganization Energy ( $\lambda$ ) for ET in Water<sup>a</sup>**

	complex in water			
	total	isoalloxazine rings	water	D-ribitol-5-phosphate
$\Delta A^\circ$	2.2 (4.0)	7.0	2.2	-6.9
$\lambda$	21.8 (18.3)	2.1	18.3	1.4

<sup>a</sup>According to the cDFT/MM scheme used in this work, the contributions from the isoalloxazine moieties are calculated at the DFT level while the other contributions are calculated at the MM level. Values in brackets are those obtained with the AMBER ff02.r1 polarizable force field. All the energies are given in kcal/mol.

Figure 6. The total driving force is almost neutral (2.2 kcal/mol). This value results from the compensation of two opposite contributions. Isoalloxazine cycles disfavors ET (7 kcal/mol) while the contribution of the ribitol-phosphate tails of the FMN favors ET (-6.9 kcal/mol). Note that water makes only a moderate contribution to  $\Delta A^\circ$ . This positive contribution of the isoalloxazine cycles can be interpreted as a preference for pairing two electrons on the same FMN while the negative contribution of D-ribitol-phosphate tails is mostly due to classical electrostatic repulsion between the negative charge of isoalloxazine rings and phosphate groups. The rotation around the N10-D-ribitol tail bond is highly energetic and does not occur during the time scale of our dynamics, but phosphate

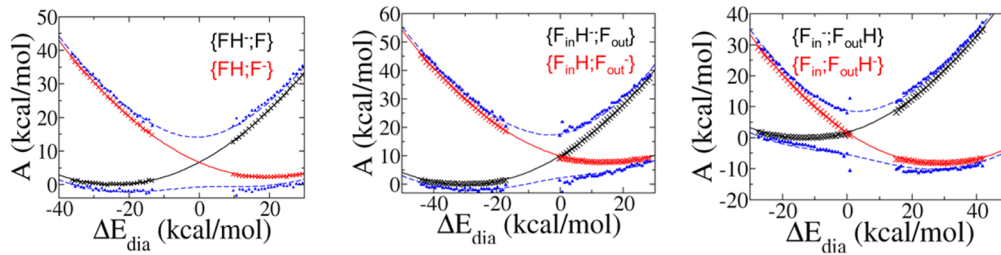


**Figure 6.** Free energy profile for the ET between stacked  $\text{FH}^{-\circ}$  and F taking the diabatic energy gap as the reaction coordinate (using the nonpolarizable force field). Points obtained from simulation data are represented by crosses (diabatic states) or by triangles (adiabatic states). The red and black solid lines are the harmonic parabolas fitting the simulation points. The blue-dashed lines are the fitted adiabatic curves. Left: FMN cofactors in water (in water the in and out subscripts are dropped). Middle and right: ET from  $\text{F}_{\text{in}}$  to  $\text{F}_{\text{out}}$  before (middle) and after (right) HAT in the EmoB protein.

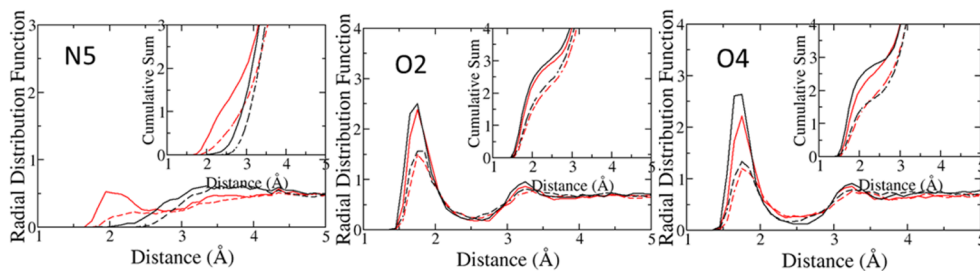


**Figure 7.** Radial distribution function of water hydrogen atoms around N5, O2, and O4 atom of the isoalloxazine rings and their cumulative sums for different states of flavins: neutral (dashed line) or negatively charged (solid line), protonated (black) or deprotonated (red).

groups are asymmetrically distributed around isoalloxazine rings: one moves between the planes containing isoalloxazine rings and does not contribute to the free energy while the other remains under the FH plane so it interacts differently with the isoalloxazine rings depending on the negative charge distribution. When employing the AMBER polarizable force field,  $\Delta A^\circ$  amount to 4 kcal/mol. However, due to the nonadditivity of polarizable FF it is not possible to decompose the contribution arising from the various components of the system.

The total reorganization energy is significant and amount to around 22 or 18 kcal/mol with the nonpolarizable and polarizable force fields, respectively. Decrease of the reorganization energy when adding electronic polarization is a common, though not systematic effects already described in the literature.<sup>15</sup> The total reorganization energy is essentially due to the aqueous environment. The radial distribution functions of the water hydrogen atoms around the N5, O2, or O4 atoms of the FMN (Figure 7) help to understand this result. For the N5 atom, a structural peak is found only for the  $\text{F}^-$  state at around 3 Å. This peak integrates to one hydrogen atom. For the isoalloxazine rings in the other electronic states this peak is less pronounced and integrates to a smaller average number of hydrogen atoms. For the O2 and O4 oxygen atoms, two types of structure of the first solvation shell are found, depending on the neutral or anionic character of the flavin. The first peak, at 2.8 Å, is higher for the anionic species ( $\text{FH}^-$  or  $\text{F}^-$ ) and integrates roughly to one more water molecule than in neutral cases. Kiliç and Ensing reported qualitatively similar behavior for isolated lumiflavin.<sup>7</sup> The differences between our profiles and the previous ones may be due to methodology (ab initio BOMD vs classical force field), simulation time length (tens of picoseconds vs hundreds of nanoseconds), and also come from the fact that we are simulating dimers of FMN and not isolated lumiflavins in water. The qualitative consistency

between our results and the first-principles radial distribution functions of Kiliç and Ensing<sup>7</sup> is encouraging for the ability of our classical FF parameters to describe the solvation shells of the FMN cofactors.

The free energy of activation  $\Delta A^{\circ\ddagger}$  calculated as  $(\Delta A^\circ + \lambda)^2 / 4\lambda$  is 6.6 kcal/mol. Over the range of the sampled  $\Delta E$ , we find that the electronic coupling remains almost constant (5–10 kcal/mol) and is of the same order as the free energy of activation. As a result the adiabatic energy curves (blue curves in Figure 6) show that no activation barrier is present for transferring the electron from one FMN to another. In addition, as already seen on the diabatic curves, the electron is almost equally stabilized on each FMN in water.

**II.2. ET and HAT within EmoB.** We now turn our attention to the EmoB protein. As already said, the FMN cofactor ( $\text{F}_{\text{in}}$ ) holding the hydride anion in the reactant state is firmly anchored to the protein by several hydrogen bonds between the FMN phosphate groups and a loop of polar residues (serine, threonine, and asparagine with residue numbers ranging from 11 to 18, Figure 1) and between the ribitol moiety of FMN and the protein backbone. Various interactions are also present with the FMN isoalloxazine group. The isoalloxazine tricycle is  $\pi$ -stacked with the Tyr80 phenol group on one side while the other side emerges at the surface of the protein and is exposed to the solvent. The oxidized FMN cofactor ( $\text{F}_{\text{out}}$ ) is positioned above (Figure 1). The protein was solvated in a water box of dimensions  $70 \times 70 \times 60 \text{ \AA}^3$ . In contrast to ET in water, the structure of the  $\pi$ -stacking between the isoalloxazine rings remains stable for hundreds of nanoseconds, and no restraints on the interflavins distances were needed to prevent destacking. These results already point toward a role of the protein matrix for favoring the interactions between the FMNs in adequate respective positions for hydrogen transfer.

We consider the energy profiles for ET before and after HAT (Figure 6, middle and right panels). For each case and for each

**Table 2. Driving Force  $\Delta A^\circ$  and Reorganization Energy  $\lambda$  in kcal/mol of the Electron Transfer between the Two Stacked Flavins in the EmoB Protein before and after Hydrogen Atom Transfer (HAT)<sup>a</sup>**

	before HAT					
	total	isoalloxazine rings	solvent	protein	D-ribitol-5-phosphate	ions
$\Delta A^\circ$	7.7 (7.04)	9.6	-14.8	19.4	-6.0	-0.5
$\lambda$	22.1 (23.6)	4.3	12.3	1.8	3.8	0.0
	after HAT					
	total	isoalloxazine rings	solvent	protein	D-ribitol-5-phosphate	ions
$\Delta A^\circ$	-8.2 (1.2)	-7.0	-10.6	15.2	-5.8	-0.3
$\lambda$	20.7 (17.1)	2.1	13.9	2.3	1.9	0.2

<sup>a</sup>The contributions from the inner part (determined at the QM level) and the outer part separated into contribution from water molecules (solvent), EmoB protein, D-ribitol-5-phosphate tail and Na<sup>+</sup> ions (ions) are also detailed. Values in brackets are those obtained with the AMBER ff02.r1 polarizable force field.

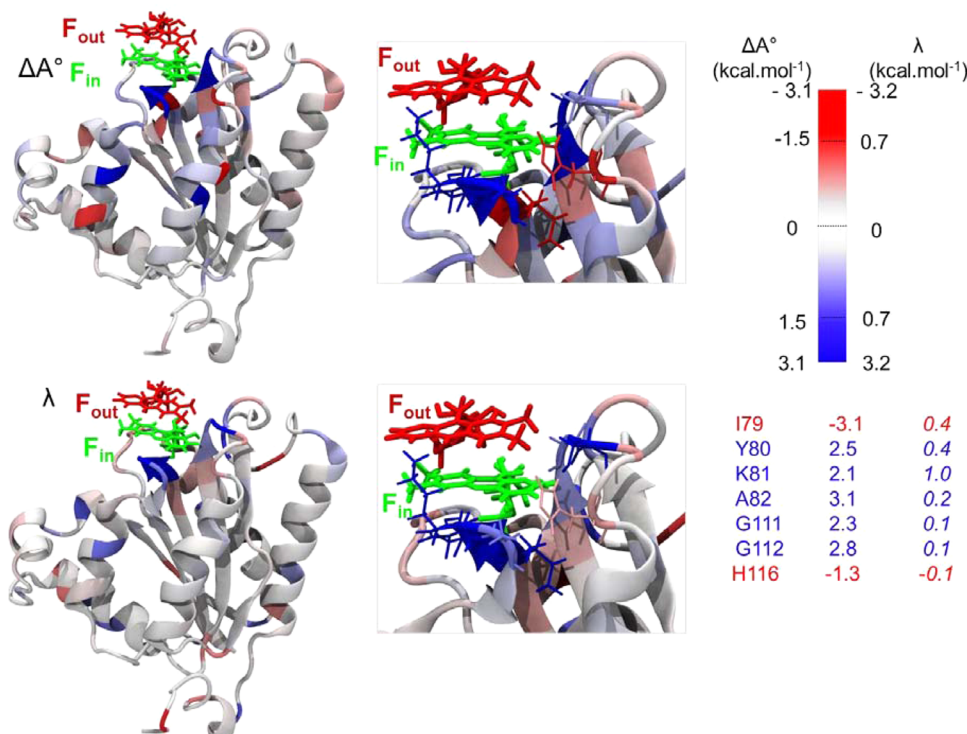


**Figure 8.** EmoB residues colored as a function of their contributions to the Gibbs free energy (top) or to the reorganization energy (bottom) and values of these contributions (normal font for  $\Delta A^\circ$  and italic for  $\lambda$ ) for some residues around the flavins (values after HAT). The figures have been drawn with VMD.<sup>5</sup>

diabatic state, two simulations of 100 ns have been performed with different initial velocities. The energy gap and the electronic coupling have been evaluated in a second step at the cDFT/MM level on snapshots extracted from the MD simulations every 100 ps. Each diabatic curve plotted in Figure 6 has thus been obtained from two thousand snapshots. It has to be noted that the mean energy gap reaches a plateau with the simulation lengths after few tens of nanoseconds (Supporting Information Figure S1). This justifies our strategy to resort to classical MD simulation for simulating the protein motions beyond the picoseconds time scale. In water, the convergence was achieved more rapidly. The Gaussian shapes of the vertical energy gap distributions (Supporting Information Figure S2) suggest that a linear approximation is again acceptable for the ET in the protein. The ET driving forces and reorganization energies are reported in Table 2.

The thermodynamic balance for ET between the FMN cofactors favors the localization of the electron on the FMN

that holds the hydrogen atom by around 8 kcal/mol (Figure 6). By comparison with the aqueous environment, it is apparent that the protein–water molecular fragments create an environment making HAT and ET dependent: before HAT, the electron remains on F<sub>in</sub>, while after HAT, it is better stabilized on F<sub>out</sub>. In other words, ET occurs if and only if HAT takes place first. The conclusion is less clear with the driving forces obtained with the polarizable FF: before HAT  $\Delta A^\circ$  is similar to that obtained with the nonpolarizable FF (ca. 7.4 kcal/mol), but it becomes only slightly positive after HAT while it was negative with the nonpolarizable FF. Actually, it is difficult to say which set of values are the most relevant (polarizable or not) because both rely on a large number of parameters. On one hand the polarizable force field may be thought as more reliable because electronic polarization is taken into account explicitly in the energy calculations. On the other hand, nonpolarizable FFs already include a part of electronic polarization (in an average way) since they are calibrated to

reproduce experimental observables. The use of the flexible SPC model for water may also enable capturing a reasonable part of the electronic polarization. The correct values are probably between those provided by the polarizable and nonpolarizable FF.

The contributions reported in Table 2 provide an explanation for the values obtained with the nonpolarizable FF. We note that contributions for the isoalloxazine rings and the d-ribitol-5 phosphate tail are similar to those found in water. In addition sodium ions do not contribute to  $\Delta A^\circ$ . On the other hand the protein and the bulk of water molecules have opposite effects on the free energies. The water molecules systematically favor the electron on  $F_{\text{out}}$ , while the protein systematically favors the electron on  $F_{\text{in}}$ . Figure 8 allows a more in-depth understanding of the effect of the protein. On this figure, the residues are colored according to their contributions to the driving force, considering the ET after HAT. The contributions are globally small (no more than 3 kcal/mol). Regarding the residues of the active site, only neutral polar moieties interact with isoalloxazine rings but they represent the greatest part of the protein contribution, while remote charged residues are close to an oppositely charged group(s) and their global interaction with flavin cores is negligible.

On the contrary, the EmoB protein does not contribute a lot to the reorganization energy (about 10%) whereas water molecules have the same behavior around  $F_{\text{out}}$  as in the uniform aqueous environment (see Supporting Information Figure S3). Contributions from each residue to reaction and reorganization free energies are determined and reported in Figure 8. As in water, the mean electronic coupling values are of the same order as the driving force (8 kcal/mol). The blue curves in Figure 6 clearly indicate the absence of a minimum on the adiabatic free energy surfaces for localizing the electron on the flavin that does not hold the hydrogen atom. This conclusion holds for both the polarizable and nonpolarizable FF results.

**II.3. Free Energy Profile for HAT.** In the previous section, we have analyzed the thermodynamics of the ET from  $F_{\text{in}}$  to  $F_{\text{out}}$  as a function of the position of the hydrogen atom. It has been found that, in EmoB, the transfer of a second electron should accompany the motion of the hydrogen atom, in an adiabatically manner. Under these conditions the HAT between the flavin is expected to be the slowest event, which now needs to be simulated. Simulation of proton or hydrogen atoms may be achieved by various computational means depending on the physicochemical framework of reference. One possibility is to follow a similar strategy as for ET and try to build free energy profiles using a solvent (environment) reaction coordinate. Physicochemical theories for dealing with proton and hydrogen atom transfer reactions have been established for a long time.<sup>6,50–52</sup> This approach is particularly useful in the case of proton transfers to account for the role of the environment fluctuations on the reaction coordinate, (as for ET reactions) and for quantum tunneling effects. In the case of hydrogen atom transfer, since the transferred particle is neutral, environment effects are far less important and other theories such as transition state theory may be adequate. The free energy profile of the formal hydride transfer has been obtained as a potential of mean force (PMF) using umbrella sampling<sup>53</sup> on the antisymmetric combination of breaking and forming bonds involving the two NS–H<sub>T</sub> distances as a reaction coordinate. The PMF curve has been calculated at the SCC-DFTB/MM level using the SCC-DFTB module of the CHARMM software.<sup>54</sup> 61 windows have been considered to

establish the PMF. For each window, a 500 ps MDS (100 ps for equilibration and 400 ps for data accumulation) has been performed constraining the reaction coordinate by a parabolic potential with a force constant of 600 kcal/mol·Å<sup>2</sup> from −1.5 Å to 1.5 Å. The time step for propagating the equations of motion was set to 0.5 fs. The weighted histogram analysis method (WHAM)<sup>55</sup> has been then used on this coordinate to get the free energy at the SCC-DFTB/MM level.

The free energy profile for the hydride transfer is showed in Figure 9. The free energy balance is neutral within the

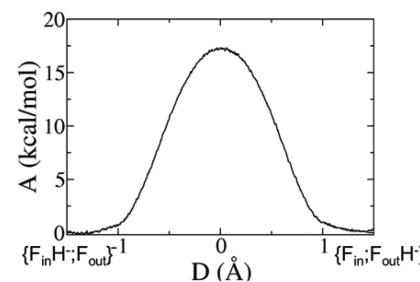


**Figure 9.** Free energy profile for the HAT between  $F_{\text{in}}$  and  $F_{\text{out}}$  in the EmoB protein.  $D$  is the antisymmetric combination of the two NS–H<sub>T</sub> distances.

uncertainty of the SCC-DFTB/MM method. A free energy barrier of around 17 kcal/mol is found. This value is consistent with typical values expected for biological net hydride transfers.<sup>56,57</sup> Even though tunneling may enhance the rate for HAT (but to a negligible extent as deduced from the application of the Bell correction<sup>58</sup> to the energy profile of Figure 9), this result confirms that HAT must be the rate limiting event in the overall formal hydride transfer. The question of the time-scale during which the FMN cofactors remain π-staked before separation is another element that has to be considered. In water, our MD simulations have shown that destacking or rearrangements of the isoalloxazine cycles take place in a few nanoseconds. The protein matrix seems to slow down such geometrical changes, since separation of the FMN cofactors has not been observed in our MD simulations of the protein (except at the very end of one simulation). Therefore, the departure of the diffusible FMN is likely to take place sometimes before the hydrogen atom has time to transfer. In such cases, however, thanks to the unfavorable thermodynamic balance for the ET from  $F_{\text{in}}$  to  $F_{\text{out}}$  (in the protein), the risk that  $F_{\text{out}}$  leaves the protein under a semireduced form is unlikely. By modulating the thermodynamic balance of ET as a function of the location of the hydrogen atom, the protein–water environment creates a mechanism to avoid “electron leakage” from the FMNH<sup>−</sup> cofactor.

## CONCLUSION

In this work, we have been interested in the analysis of the formal hydride transfer between two FMN cofactors positioned at the surface of the EmoB protein. We have been working in the framework of the Marcus theory to determine the energy profiles of the ET between the FMN cofactors as a function of the position of the hydrogen atom. The energy profiles have been calculated according to well established protocols, although one innovation of the present work is to make use of the constrained DFT approach proposed by Dederichs et al.<sup>22</sup> and Wu et al.<sup>23</sup> to define ad hoc diabatic states, to calculate their energies and to extract the coupling between them.

The transfer of the hydrogen atom between the N5 atoms was found to be rate limiting in the protein, with the transfer of the second electron transferring adiabatically from the inner to the outer FMNs. The contributions of the different fragments to the free energy of the ET reactions and to the reorganization were examined. The fact that hydrogen transfer is rate limiting, compared to electron transfer, was rather expected because the electronic coupling between the ET diabatic states is significant. On the other hand, we may find other biological systems where the electronic coupling might be smaller because of the distance between the donor and the acceptor, or for symmetry reason. Coming back to the EmoB system, the principal outcome of our study is to highlight the role of the protein in intertwining the transfers of the electron and of the hydrogen atom. Compared to the aqueous environment in which the process is thermodynamically and kinetically favorable to achieve a one electron reduction of the nonprotonated FMN, in EmoB, the transfer of the electron was found to be unfavorable (by 8 kcal/mol) unless the hydrogen atom transfer takes place. After HAT, ET becomes favorable by 8 kcal/mol with the CHARMM force field. The polarizable and nonpolarizable FF provided very similar results except for the stabilization of the final  $\{F_{in}; F_{out}H^-\}$ , which is less stabilized with polarizable FF (1.2 vs -8 kcal/mol).

The transfer of the hydrogen atom is rather slow compared to ET given the large free energy of activation (17 kcal/mol), and probably to the loss of the noncovalent  $\pi$ -stacked interactions between the flavins, there is potential risk to have a one electron reduction of the outer FMN without transfer of the hydrogen atom. Such processes would produce radical flavins instead of the fully reduced FMN required by the protein EmoA. The thermodynamic coupling between ET and HAT in the EmoB protein avoids such a risk. This conclusion therefore supports the hydride carrier role assigned to the EmoB protein in the *Mesorhizobium* species. The decomposition of the driving force into contributions from the different residue suggest that mutagenesis of residues situated few angstroms away from  $F_{in}$  could be introduced to favor ET before the hydrogen atom take places. For example, the introduction of negatively charged residues should lead to smaller  $\Delta A^\circ$  before HAT takes place and, therefore, one electron reduction of the outer flavin, with no HAT. Alternatively, positively charged residues could help retaining the second electron on the protein flavin ( $F_{in}$ ) even if the transfer of the hydrogen atom has taken place. Such experiments would allow investigating more in depth the hydride transfer mechanism in EmoB or other hydride carrier proteins.

## ASSOCIATED CONTENT

### Supporting Information

Constrained DFT with various population analyses approaches. Force field parameter for the dimers of flavins, convergence tests of the diabatic energy gaps. This material is available free of charge via the Internet at <http://pubs.acs.org>.

## AUTHOR INFORMATION

### Corresponding Authors

\*Email: natacha.gillet@u-psud.fr.

\*Email: aurelien.de-la-lande@u-psud.fr.

### Notes

The authors declare no competing financial interest.

## ACKNOWLEDGMENTS

We are grateful to Compute Canada/WestGrid for the provision of substantial High-Performance Computing resources and to the French Computer Centers (CINES, project number c2014076913). V.M. thanks the Spanish Ministry of Economy and Competitiveness (CTQ2012-36253-C03-01) and Universitat Jaume I (P1·1B2011-23) for financial support. We are grateful to Jacqueline Ridard for her valuable help in preparing AMBER calculations.

## REFERENCES

- (1) Weinberg, D. R.; Gagliardi, C. J.; Hull, J. F.; Murphy, C. F.; Kent, C. A.; Westlake, B. C.; Paul, A.; Ess, D. H.; McCafferty, D. G.; Meyer, T. *J. Chem. Rev.* **2012**, *112*, 4016–4093.
- (2) Nagel, Z. D.; Klinman, J. P. *Chem. Rev.* **2006**, *106*, 3095–3118.
- (3) Bohuslavek, J.; Payne, J. W.; Liu, Y.; Bolten, J. R., Jr.; Xun, L. *Appl. Environ. Microbiol.* **2001**, *67*, 688–695.
- (4) Nissen, M. S.; Youn, B.; Knowles, B. D.; Ballinger, J. W.; Jun, S.-Y.; Becchik, S. M.; Xun, L.; Kang, C. *J. Biol. Chem.* **2008**, *283*, 28710–28720.
- (5) Humphrey, W.; Dalke, A.; Schulten, K. *J. Mol. Graphics* **1996**, *14*, 33–38.
- (6) Hammes-Schiffer, S. *Energy Environ. Sci.* **2012**, *5*, 7696–7703.
- (7) Layfield, J. P.; Hammes-Schiffer, S. *Chem. Rev.* **2014**, *7*, 3466–3494.
- (8) Yu, T.; Higashi, M.; Cembran, A.; Gao, J.; Truhlar, D. G. *J. Phys. Chem. B* **2013**, *117*, 8422–8429.
- (9) Kiliç, M.; Ensing, B. *J. Chem. Theory Comput.* **2013**, *9*, 3889–3899.
- (10) Mueller, R. B.; North, M. A.; Yang, C.; Hati, S.; Bhattacharyya, S. *J. Phys. Chem. B* **2011**, *115*, 3632–3641.
- (11) Marcus, R. A.; Sutin, N. *Biochim. Biophys. Acta* **1985**, *811*, 265–322.
- (12) Warshel, A. *J. Phys. Chem.* **1982**, *86*, 2218–2224.
- (13) King, G.; Warshel, A. *J. Chem. Phys.* **1990**, *93*, 8682–8692.
- (14) Cheng, J.; Sulpizi, M.; Sprik, M. *J. Chem. Phys.* **2007**, *131*, 154504–20.
- (15) Blumberger, J. *Phys. Chem. Chem. Phys.* **2008**, *10*, 5651–5667.
- (16) Marcus, R. A. *J. Chem. Phys.* **1965**, *43*, 679–701.
- (17) Hwang, J.-K.; Warshel, A. *J. Am. Chem. Soc.* **1987**, *109*, 715–720.
- (18) Bhattacharyya, S.; Stankovich, M. T.; Truhlar, D. G.; Gao, J. *J. Phys. Chem. A* **2007**, *111*, 5729–5742.
- (19) Hu, L.; Farrokhnia, M.; Heimdal, J.; Shleev, S.; Rulišek, L.; Ryde, U. *J. Phys. Chem. B* **2011**, *115*, 13111–13126.
- (20) Tachiya, M. *J. Chem. Phys.* **1989**, *93*, 7050–7052.
- (21) Tachiya, M. *J. Chem. Phys.* **1993**, *97*, 5911–5916.
- (22) Dederichs, P. H.; Blügle, S.; Zeller, R.; Akai, H. *Phys. Rev. Lett.* **1984**, *53*, 2512–2515.
- (23) Wu, Q.; Van Voorhis, T. *Phys. Rev. A* **2005**, *72*, 024502–024506.
- (24) Kaduk, B.; Kowalczyk, T.; Van Voorhis, T. *Chem. Rev.* **2012**, *112*, 321–370.
- (25) de la Lande, A.; Salahub, D. R.; Köster, A. M. Extending the Application of Constrained Density Functional Theory to Large Molecular Systems. In *Concepts and Methods in Modern Theoretical Chemistry: Electronic Structure and Reactivity*; Ghosh, S. K., Chattaraj, P. K., Eds.; Taylor and Francis: New York, 2012.
- (26) Köster, A. M.; Calaminici, P.; Casida, M. E.; Flores-Moreno, R.; Geudtner, G.; Goursot, A.; Heine, Th.; Ipatov, A.; Janetzko, F.; del Campo, J. M.; Patchkovskii, S.; Ulises Reveles, J.; Salahub, D. R.; Vela, A. *deMon2k*, Version 2; Cinvestav: Mexico City, 2006.
- (27) (a) de la Lande, A.; Salahub, D. R. *J. Mol. Struct. THOECHEM* **2010**, *1*, 115–120. (b) Řezáč, J.; Lévy, B.; Demachy, I.; de la Lande, A. *J. Chem. Theory Comput.* **2012**, *8*, 418–427.
- (28) Köster, A. M.; Reveles, J. U.; del Campo, J. M. *J. Chem. Phys.* **2004**, *121*, 3417.

- (29) Perdew, J. P.; Burke, K.; Ernzerhof, M. *Phys. Rev. Lett.* **1996**, *77*, 3865.
- (30) (a) Krack, M.; Köster, A. M. *J. Chem. Phys.* **1998**, *108*, 3226–3234. (b) Köster, A. M.; Flores-Moreno, R.; Ulises Reveles, J. *J. Chem. Phys.* **2004**, *121*, 681–690.
- (31) Köster, A. M. *J. Chem. Phys.* **2003**, *118*, 9943–9951.
- (32) Calaminici, P.; Janetzko, F.; Köster, A. M.; Mejia-Olvera, R.; Zuniga-Gutierrez, B. *J. Chem. Phys.* **2007**, *126*, 044108.
- (33) Goursot, A.; Mineva, T.; Kevorkyants, R.; Talbi, D. *J. Chem. Theory Comput.* **2007**, *3*, 755–763.
- (34) Wu, Q.; Yang, W. *J. Chem. Phys.* **2002**, *116*, 515–524.
- (35) Warshel, A.; Levitt, M. *J. Mol. Biol.* **1976**, *103*, 227–249.
- (36) Vreven, T.; Byun, K. S.; Kom-romi, I.; Dapprich, S.; Montgomery, J. A.; Morokuma, K.; Frisch, M. J. *J. Chem. Theory Comput.* **2006**, *2*, 815–826.
- (37) Brooks, B. R.; Brooks, C. L.; Mackerell, A. D., Jr.; Nilsson, L.; Petrella, R. J.; Roux, B.; Won, Y.; Archontis, G.; Bartels; Boresch, S.; Caflisch, A.; Caves, L.; Cui, Q.; Dinner, A. R.; Feig, M.; Fischer, S.; Gao, J.; Hodoscek, M.; Im, W.; Kuczera, K.; Lazaridis, T.; Ma, J.; Ovchinnikov, V.; Paci, E.; Pastor, R. W.; Post, C. B.; Pu, J. Z.; Schaefer, M.; Tidor, B.; Venable, R. M.; Woodcock, H. L.; Wu, X.; Yang, W.; York, D. M.; Karplus, M. *J. Comput. Chem.* **2009**, *30*, 1545–1614.
- (38) Fanfrlík, J.; Brynda, J.; Řezáč, J.; Hobza, P.; Lepšík, M. *J. Phys. Chem. B* **2008**, *112*, 15094–15102.
- (39) Wu, Q.; Van Voorhis, T. *J. Chem. Phys.* **2006**, *125*, 164105–164113.
- (40) Gehlen, J. N.; Chandler, D.; Kim, H. J.; Hynes, J. T. *J. Phys. Chem.* **1992**, *96*, 1748–1753.
- (41) Zhao, X. G.; Cukier, R. I. *J. Phys. Chem.* **1995**, *99*, 945–954.
- (42) Cieplak, P.; Dupradeau, F.-X.; Duan, Y.; Wang, J. *J. Phys.: Condens. Matter* **2009**, *21*, 333102–333123.
- (43) Ji, C.; Changge; Mei, Y. *Acc. Chem. Res.* **2014**, DOI: 10.1021/ar500094n.
- (44) Wang, Z. X.; Zhang, W.; Wu, C.; Lei, H.; Cieplak, P.; Duan, Y. *J. Comput. Chem.* **2006**, *27*, 781–790.
- (45) Li, H.; Robertson, A. D.; Jensen, J. H. *Proteins* **2005**, *61*, 704–721. Bas, D. C.; Rogers, D. M.; Jensen, J. H. *Proteins* **2008**, *73*, 765–783. Olsson, M. H. M.; Søndergaard, C. R.; Rostkowski, M.; Jensen, J. H. *J. Chem. Theory Comput.* **2011**, *7*, 525–537. Søndergaard, C. R.; Olsson, M. H. M.; Rostkowski, M.; Jensen, J. H. *J. Chem. Theory Comput.* **2011**, *7*, 2284–2295.
- (46) Wu, Y.; Tepper, H. L.; Voth, G. A. *J. Chem. Phys.* **2006**, *124*, 024503.
- (47) Singh, U. C.; Kollman, P. A. *J. Comput. Chem.* **1984**, *5*, 129–145.
- (48) Bayly, C. I.; Cieplak, P.; Cornell, W.; Kollman, P. A. *J. Phys. Chem.* **1993**, *97*, 10269–10280.
- (49) Phillips, J. C.; Braun, R.; Wang, W.; Gumbart, J.; Tajkhorshid, E.; Villa, E.; Chipot, C.; Skeel, R. D.; Kale, L.; Schulten, K. *J. Comput. Chem.* **2005**, *26*, 1781–1802.
- (50) Borgis, D.; See, S.; Hynes, C. *Chem. Phys. Lett.* **1989**, *162*, 19–26.
- (51) Morillo, M.; Cukier, R. I. *J. Chem. Phys.* **1990**, *92*, 4833–4838.
- (52) Cukier, R. I.; Nicera, G. G. *Annu. Rev. Phys. Chem.* **1998**, *49*, 337–369.
- (53) Torrie, G. M.; Valleau, J. P. *J. Comput. Phys.* **1977**, *23*, 187–199.
- (54) Cui, Q.; Elstner, M.; Kaxiras, E.; Frauenheim, T.; Karplus, M. *J. Phys. Chem. B* **2001**, *105*, 569–585.
- (55) Kumar, S.; Bouzida, D.; Swendsen, R. H.; Kollman, P. A.; Rosenberg, J. M. *J. Comput. Chem.* **1992**, *13*, 1011–1021.
- (56) Kong, Y. S.; Warshel, A. *J. Am. Chem. Soc.* **1995**, *117*, 6234–6242.
- (57) Lans, I.; Medina, M.; Rosta, E.; Hummer, G.; Garcia-Viloca, M.; Lluch, J. M.; González-Lafont, A. *J. Am. Chem. Soc.* **2012**, *134*, 20544–20553.
- (58) Limbach, H. –H.; Lopez, J. M.; Kohen, A. *Phil. Trans. Roy. Soc. B* **2006**, *361*, 1399–1415.